JOURNAL OF AIRCRAFT
Vol. 44, No. 4, July–August 2007

Evaluation of a Simplified Grid Treatment for Oscillating Trailing-Edge Control Surfaces

A. M. Rampurawala* and K. J. Badcock†
University of Liverpool, Liverpool, L3 9TY England, United Kingdom

DOI: 10.2514/1.24623

The aeroelastic behavior associated with control surfaces is of particular practical interest. The treatment of the control surface in a computational fluid dynamics based simulation is complicated by the change in topology of the geometry as the flap edge is exposed. This paper evaluates the use of a treatment which blends the flap edge into the wing. This simplifies the mesh treatment by avoiding topological changes. The influence of the treatment of the forced flap motions on the aerodynamic responses of the rigid benchmark active control technology wing and a flexible supersonic transport wing is evaluated. Comparison is made with results obtained when the flap edge is exposed. It is shown that the predictions from the blended treatment give similar results, including local effects on the control surface, to calculations which include the flap edge effects.

Nomenclature

$\boldsymbol{f}$	=	force acting at the grid points
$\boldsymbol{K}$	=	structural stiffness matrix
$\boldsymbol{M}$	=	structural mass matrix
M_∞	=	freestream Mach number
$\boldsymbol{x}$	=	grid locations
δ	=	change in grid locations
δ_f	=	flap angle
η	=	generalized modal coordinates
ψ_i^0	=	blending function for transfinite interpolation
ω	=	modal frequency

Subscripts

a	=	aerodynamic surface grid
s	=	structural grid

Introduction

IT IS important that control surfaces are free of any structural or aerodynamic instabilities. Instability can be encountered at transonic Mach numbers when the shock moves over the trailing-edge control surface. This can lead to oscillations of the control surface and is an issue for supersonic transport aircraft with thin trailing-edge flaps because the lack of space can prevent adequate constraints being applied. The first recorded case of a buzz incident was on the P-80 jet fighter which encountered low amplitude oscillations at transonic Mach numbers in 1945 [1]. Permanent damage was caused to the aileron as the buzz amplitude increased when the aircraft flew at higher Mach numbers. It was later identified by Lambourne [2] as a shock induced instability. There have been numerous cases of buzz since then as aircraft flew in the transonic regime. However with the introduction of hydraulic actuators buzz became less of a problem. The most recent case was reported on the T45 Goshawk aircraft which suffered from rudder buzz during a flight test program [3].

Another aeroelastic phenomenon associated with trailing-edge control surfaces is that of aileron reversal which has implications on the wing design [4]. It is stated [5] that for the case of a supersonic transport (SST) at Mach 1, the effectiveness of the aileron was reduced to zero due to aeroelastic effects. An interesting example is of the F-18 fighter aircraft which suffered from aileron reversal. The wing torsional flexibility which caused the reversal was later used as a means of morphing the wings for roll maneuvers. This was successfully tested in the active aeroelastic wing (AAW) project at NASA Dryden on the F-18 high alpha research vehicle (HARW).

One of the first computational forced flap oscillation studies was performed by Bharadvaj [6] on the F5 and HARW rigid wing configurations. This computational analysis used the transonic full potential equations to calculate the unsteady loads due to the forced flap oscillations. The control surface deflections were brought about by an equivalent body velocity that changes the boundary conditions to model the effect of a moving control surface. The viscous effects were modeled through an interactive inverse boundary layer and the transpiration velocity approach.

The benchmark active control technology (BACT) wing has a rich database for the validation of aeroelastic and aeroservoelastic computations. Computations for unsteady pressure prediction have been performed on the BACT case by Schuster for the case with an oscillating trailing-edge control surface [7]. This case is also studied in the current paper for the purpose of validating the computational fluid dynamics (CFD) code. The treatment of the control surface by Schuster [7] is similar to the blended edge treatment BACT case of the current work. The BACT wing is extremely rigid and hence the pressure unsteadiness is due to the flap motion alone. This simplifies the aerodynamic response and makes it a good case for validating the forced flap oscillation methodology.

A transpiration boundary condition was applied to treat an oscillating flap by Cole et al. [8,9] to simulate the BACT case and the unsteady pressure distribution compared with the experiments. The basic idea is that the motion of the control surface is represented by changing the velocity boundary conditions of the grid cells over the moving surface.

Klopfer and Obayashi developed and implemented a virtual zone technique for the treatment of oscillating control surfaces. The technique uses intermediate virtual zones to act as an interface between the control surface and wing edges. The virtual zones do not have volumes and flow computations do not take place within these zones. Multiple boundary conditions can be applied to these zones [10] and hence they act as an interface between the wing edge and dynamic flap edge. This was tested for a clipped delta wing and the computed results were validated against experiments [11].

Presented as Paper 4962 at the AIAA Applied Aerodynamics Conference, Toronto; received 15 April 2006; revision received 18 February 2007; accepted for publication 20 February 2007.

*Postgraduate Student, Computational Fluid Dynamics Laboratory, Flight Sciences and Technology, Department of Engineering.

†Professor, Computational Fluid Dynamics Laboratory, Flight Sciences and Technology, Department of Engineering; K.J.Badcock@liverpool.ac.uk (Corresponding Author).

Forced flap oscillations using the unsteady Reynolds-averaged Navier–Stokes (RANS) equations were performed for the F5 wing and a clipped delta wing by Obayashi and Guruswamy using the CFD code ENSAERO [12]. The control surface deflections were modeled by shearing the grid at the control surface-wing interface for both of the cases. It was stated that the shearing of the grids at the control surface gaps gave reasonable results for small amplitude forced oscillations that were being validated. The wings were treated as rigid.

Obayashi et al. [13] analyzed a full span rigid arrow wing with symmetric and antisymmetric oscillating control surfaces. The Reynolds-averaged thin layer Navier–Stokes equations were used in this study and the interaction of the primary vortex, the wake vortex, and the flap oscillations at moderate angles of attack was demonstrated. The results were validated against wind-tunnel experiments. Gaps were introduced between the control surface and the wing with the grids within the gap sheared as the flap moves. The amplitude of flap oscillation was 8.3 deg.

The unsteady pressure distribution due to an oscillating trailing-edge control surface was calculated over a 55 deg rigid delta wing by Karlsson [14]. Results for the transonic case were calculated using linear aerodynamics, full potential, and the Euler equations and were compared with the experimental results.

All of the cases listed above were for rigid wings. As aircraft wings are flexible to some extent, a more realistic test case is for an oscillating control surface on a flexible structure. The unsteady pressure distribution over the wing due to control surface oscillations results in dynamic structural deflections. Moreover the flap oscillating frequency (FOF) may induce resonance for a natural frequency of vibration of the structure causing large deformations.

Such a simulation is performed in the current study on a flexible supersonic configuration. The Japan Aerospace Exploration Agency (JAXA) [formerly National Aerospace Laboratory (NAL)], as part of the Japanese SST program, is developing an experimental supersonic transport model and a wind-tunnel model of this was tested in the transonic regime for unsteady pressure and dynamic deformation [15,16]. The purpose of the experiment was to accumulate data for the validation of aeroelastic codes and active control technology. These experimental data are used in the current paper.

Tamayama et al. [17] performed 2-D forced flap oscillation calculations on the NAL–SST wing profile. The main objective of the study was to investigate the shock motion due to flap oscillations. A 2-D RANS code with a thin layer assumption for the boundary layer was used. The wing profile of the 2-D case was the same as the one used in the current work. A 3-D forced flap oscillation study was performed by Utaka and Nakamichi [18] on the NAL–SST configuration. The wing was modeled as elastic and the unsteady pressure coefficients were compared against the measurements. The dynamic deformation was, however, not compared. A Chimera grid approach was used to model the control surface and the Euler equations were used to model the flow.

In the current paper we are interesting in testing a simple treatment for applying a forced flap motion to a flexible wing. The computational framework uses block structured grids and it is very convenient to blend the flap into the wing. This avoids topology changes as the flap deforms and also retains the simplicity and accuracy of one-to-one grid point connectivity at the flap edges. In addition, a simple way of defining the flap motions can be used, which is described in the next section. A concern is how the flap blending alters the predictions, and this is evaluated for two test cases (the rigid BACT wing and the flexible SST wing). These cases are described in detail next, followed by results to allow the effectiveness of the blending treatment to be evaluated.

Aeroelastic Simulation

Fluid and Structural Solver

The Euler and RANS equations are discretized on curvilinear multiblock body conforming grids using a cell-centered finite volume method which converts the partial differential equations into a set of ordinary differential equations. The convective terms are discretized using Osher's [19] upwind method. The monotone upwind scheme for conservation laws (MUSCL) variable extrapolation is used to provide second-order accuracy with the Van Albada limiter to prevent spurious oscillations around shock waves. Following Jameson [20], the spatial residual is modified by adding a second-order discretization of the real time derivative to obtain a modified steady-state problem for the flow solution at the next real time step, which is solved through pseudotime. This pseudotime problem is solved using an unfactored implicit method, based on an approximate linearization of the residual. The linear system is solved in unfactored form using a Krylov subspace method with block incomplete upper–lower (BILU) preconditioning. The preconditioner is decoupled between blocks to allow a very high efficiency on parallel computers with little detriment to the convergence of the linear solver. For the Jacobian matrix of the CFD residual function, approximations are made which reduce the size and improve the conditioning of the linear system without compromising the stability of the time marching.

This formulation is implemented in the flow code parallel multiblock (PMB). The equations are solved on block structured grids. A wide variety of unsteady flow problems, including cavity flows, aerospike flows, delta wing aerodynamics, rotorcraft problems, and transonic buffet have been studied using this code. More details on the flow solver can be found in Badcock et al. [21].

The geometries of interest deform during the motion and the mesh must be moved to conform with the evolving geometry. This is achieved using transfinite interpolation (TFI) of displacements within the blocks containing the aircraft. The surface deflections are interpolated to the volume grid points $\boldsymbol{x}_{ijk}$ as

$$\delta \boldsymbol{x}_{ijk} = \psi_j^0 \delta \boldsymbol{x}_{a,ik} \tag{1}$$

where ψ_j^0 are values of a blending function (see Gordon and Hall [22]) which varies between 1 at the aircraft surface and 0 at the block face opposite. The surface deflections $\boldsymbol{x}_{a,ik}$ are obtained from the transformation of the deflections on the structural grid and so ultimately depend on the values of the generalized structural coordinate η_i (defined later). The grid speeds can be obtained by differentiating Eq. (1) to obtain their explicit dependence on the values of $\dot{\eta}_i$. A global conservation law is used to compute the volume of the deforming cells [23].

Finite element methods allow for the static and dynamic response of a structure to be determined. Stiffness $\boldsymbol{K}$ and mass $\boldsymbol{M}$ matrices are used to determine the equation of motion of an elastic structure subjected to an external force $\boldsymbol{f}_s$ as

$$\boldsymbol{M}\,\delta\ddot{\boldsymbol{x}}_s + \boldsymbol{K}\delta\boldsymbol{x}_s = \boldsymbol{f}_s \tag{2}$$

where $\delta \boldsymbol{x}_s$ is a vector of displacements on a grid of points $\boldsymbol{x}_s$. Because the structural system under consideration is assumed to be linear, its characteristics are determined once and for all before making the flutter calculations, so that $\boldsymbol{M}$ and $\boldsymbol{K}$ are constant matrices generated, in this case, by the commercial package MSC/NASTRAN.

The aircraft deflections $\delta \boldsymbol{x}_s$ are defined at a set of grid points $\boldsymbol{x}_s$ by

$$\delta \boldsymbol{x}_s = \sum \eta_i \phi_i \tag{3}$$

where ϕ_i are the mode shapes and η_i the generalized displacements. Projecting the finite element equations onto the mode shapes results in the equations

$$\frac{d^2\eta_i}{dt^2} + \omega_i^2 \eta_i = \phi_i^T \boldsymbol{f}_s \tag{4}$$

where $\boldsymbol{f}_s$ is the vector of external forces at the structural grid points. This equation can be solved by a two stage Runge–Kutta method, which requires a knowledge of $\boldsymbol{f}_s^n$ and $\boldsymbol{f}_s^{n+1}$.

Table 1 Experimental details of the BACT cases selected for current computations

	Incidence	Mean flap angle	Mach no.	FOF, Hz	Flap amplitude
Case 1	−4.02 deg	0 deg	0.769	0	0 deg
Case 2	0.03 deg	5.0 deg	0.769	0	0 deg
Case 3	0 deg	0 deg	0.766	5	2.02 deg

Table 2 Conditions of the SST cases selected for computations

	Incidence	Mean flap angle	Mach no.	FOF, Hz	Flap amplitude
Case 1	0.0 deg	0.0 deg	0.8002	10	1.203 deg
				15	1.312 deg
				20	1.116 deg
				25	1.004 deg
Case 2	−2.0 deg	0.0 deg	0.8009	10	1.567 deg
				15	1.448 deg
				20	1.229 deg
				25	1.091 deg
Case 3	−4.0 deg	5.0 deg	0.9007	5	1.844 deg
				10	1.756 deg
				20	1.284 deg

Transformation Between Fluid and Structural Grids

The constant volume tetrahedron (CVT) scheme is a transformation technique proposed by Goura [24]. Each fluid surface grid point is first associated with a triangular element on the structural grid. The projection of the fluid point onto the triangle is moved linearly with respect to the structural points. The vector connecting the projected point and the fluid surface point is rotated to keep it normal to the plane of the triangle, and the magnitude is scaled to keep the volume of the tetrahedron formed by the three structural points and the fluid point constant.

Combination of Forced and Free Motions

A feature of the response of a flexible wing to a forced control surface is that there are two contributions to the changing geometry of the problem. The first is the elastic deformation due to the changing aerodynamic forces. This is calculated on the structural grid from Eq. (3) and then transformed, using the method summarized in the previous section, to the aerodynamic surface grid. The second is due to the forced flap motion, which is imposed on the problem.

The following approach is used to allow the definition of the forced motion through an input file. First, a set of forced mode shapes are defined on the undeflected fluid surface grid by regenerating the surface grid at the maximum flap deflection. The mode shape is calculated by subtracting the deflected positions from the original values. An input file to define the flap motion is read by the code, and the forced deflection is calculated by scaling the flap mode shape by the proportion of the maximum deflection requested at that time step. This deflection is added to the structural deflections to obtain the total deflection of the surface grid.

Experimental Models

BACT Wing

The benchmark active control technology wing model was developed at NASA Langley as part of the benchmark model

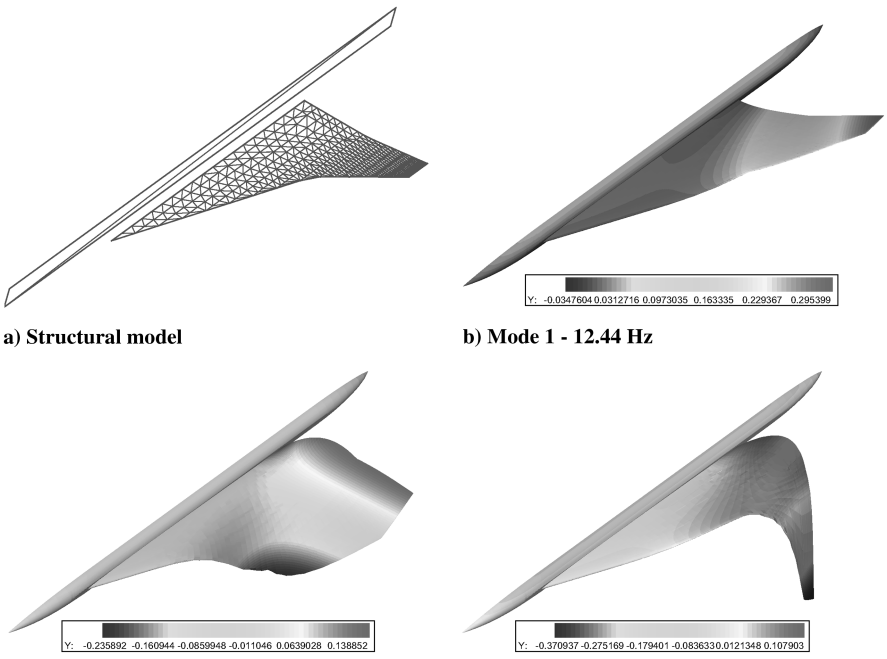

a) Structural model

b) Mode 1 - 12.44 Hz

c) Mode 2 - 51.65 Hz

d) Mode 3 - 58.32 Hz

Fig. 1 The structural model and transformed mode shapes used in the flexible SST simulations.

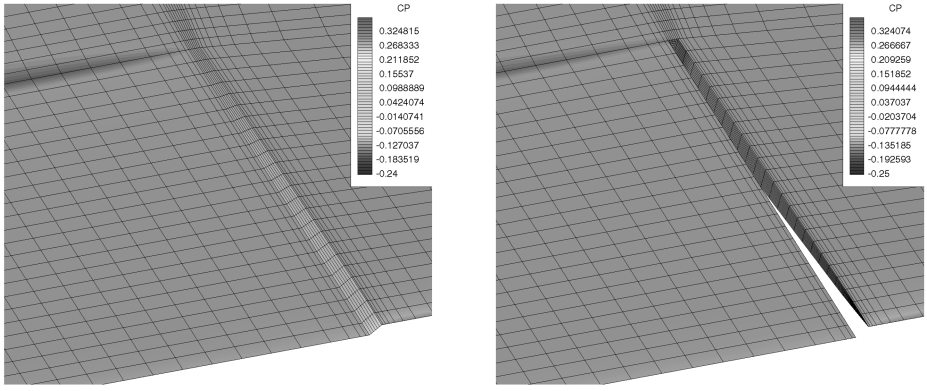

a) Cp contours on a blended flap on the SST

b) Cp contours over a flap with free edges on the SST

Fig. 2 The two types of modeling of the flap edges.

program. It is a generic rectangular wing with a NACA 0012 wing profile. It has upper and lower surface spoilers and a trailing-edge control surface which can be oscillated for use in flutter suppression and dynamic response excitation. There have been a large number of experiments performed on this model over the years including the identification of the flutter boundary when the model is mounted on a pitch and plunge apparatus (PAPA), steady and unsteady control surface effectiveness studies, and the measurement of a dynamic response of a flexible system due to control surface excitation. The experiments on forced trailing-edge control surface oscillations used in the current work were performed by Bennett et al. [25] changing a wide range of parameters like Mach number, FOFs, angle of incidence, flap deflection angles, and spoiler deflection angles. The validation data are in the form of unsteady pressure coefficient values along the entire chord at 60% span, and between 60% and 100% of the chord at 40% span, with the sensor array at 60% span running across the flap. The experimental data are in the form of mean, real, and imaginary components. The fast Fourier transform function fft in MATLAB was used to process the computed time histories at each surface grid point for comparison with measurements. The BACT wing is very rigid and does not exhibit any structural deformation due to forced flap motions.

Three experimental cases have been selected for this study. The Reynolds number based on root chord is 3.96×10^6. Details of the

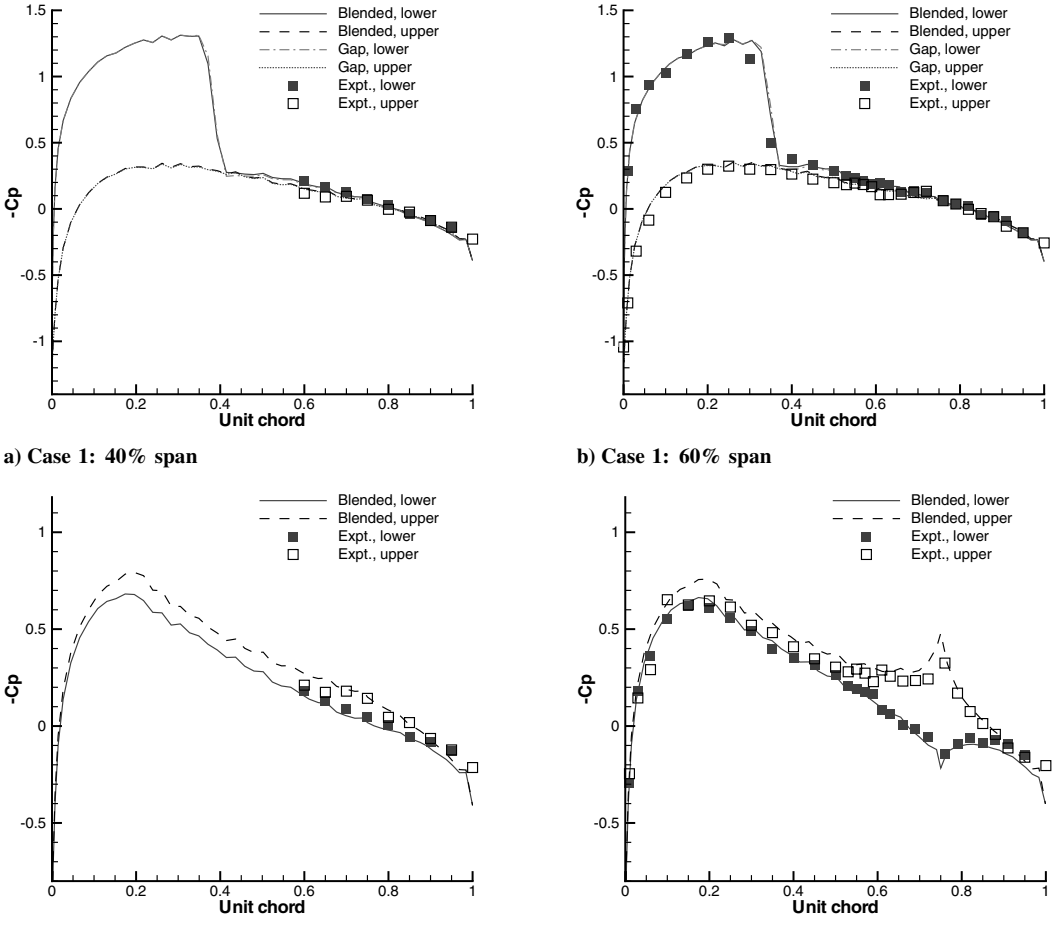

a) Case 1: 40% span

b) Case 1: 60% span

c) Case 2: 40% span

d) Case 2: 60% span

Fig. 3 BACT cases 1 and 2 steady pressure coefficient values using blended flap and flap with gaps.

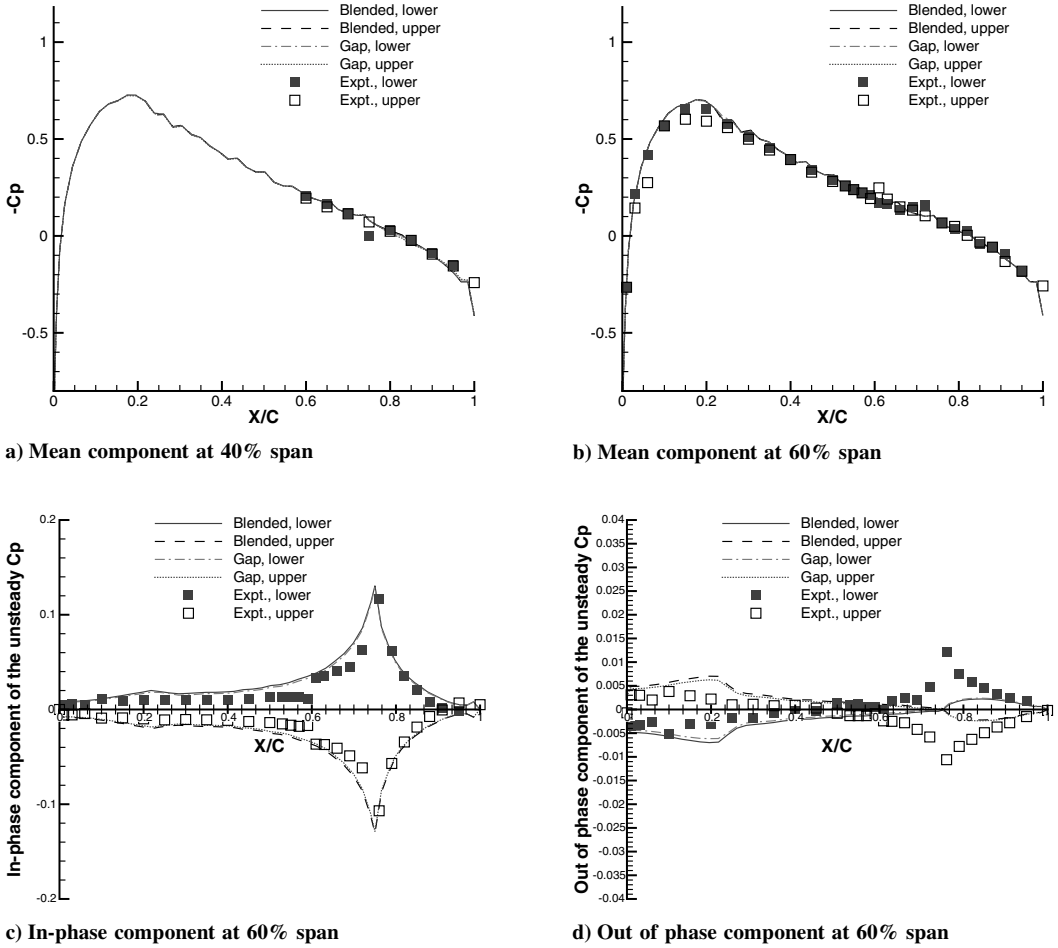

a) Mean component at 40% span

b) Mean component at 60% span

c) In-phase component at 60% span

d) Out of phase component at 60% span

Fig. 4 BACT case 3 pressure coefficient values using blended flap and flap with gaps. $M_\infty = 0.769$, $Re = 3.96 \times 10^6$, $\delta_f = 2.02$ deg.

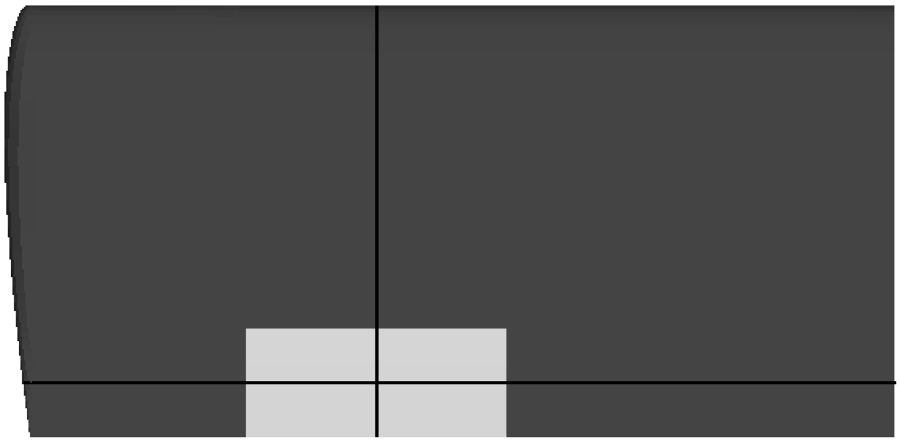

Fig. 5 BACT case 3 detail around the flap—slices used.

experiments are given in Table 1. Cases 1 and 2 are static, whereas case 3 involves forced flap oscillations.

NAL–SST Arrow Wing

The second test case is based on the transonic aeroelastic experiments performed at NAL [15]. One of the motivations for the experiments was to generate a set of results against which aeroelastic codes could be validated. For this reason, along with the unsteady pressure distribution over the wing, the dynamic deformation and unsteady force coefficients were also measured.

The SST arrow wing is a cranked double delta with a root chord of 2.103 m. A half-model was used in the experiments with a semispan of 1 m. The section profile is a NACA 0003. The inboard delta has a sweep angle of 72.8 deg and outboard the sweep is 51.6 deg. The trailing-edge flap starts at 20% half-span and terminates at 50% half-span, with a flap chord of 0.11 m. Experimental data are available for a range of Mach numbers between 0.79 and 0.91, angles of attack of 0, −2, and −4 deg, flap mean angles of 0, −5, and 5 deg, and FOFs of 5, 10, 15, 20, 25, and 30 Hz. Three cases were selected for investigation and are listed in Table 2. The unsteady pressures are validated on the upper surface at 38% span. Measurements were also obtained at 74% span but comparisons are omitted here due to lack of space, although they are included in Rampurawala [26]. The slice at 38% span runs through the flap with the hinge located at 90.5% of the local chord. Distinct peaks on the unsteady pressure can be seen

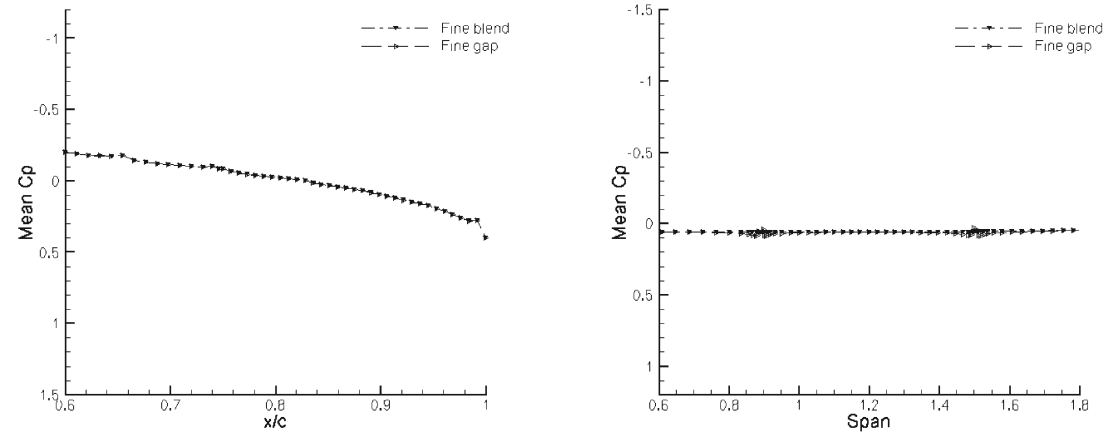

a) Mean component - streamwise

b) Mean component - spanwise

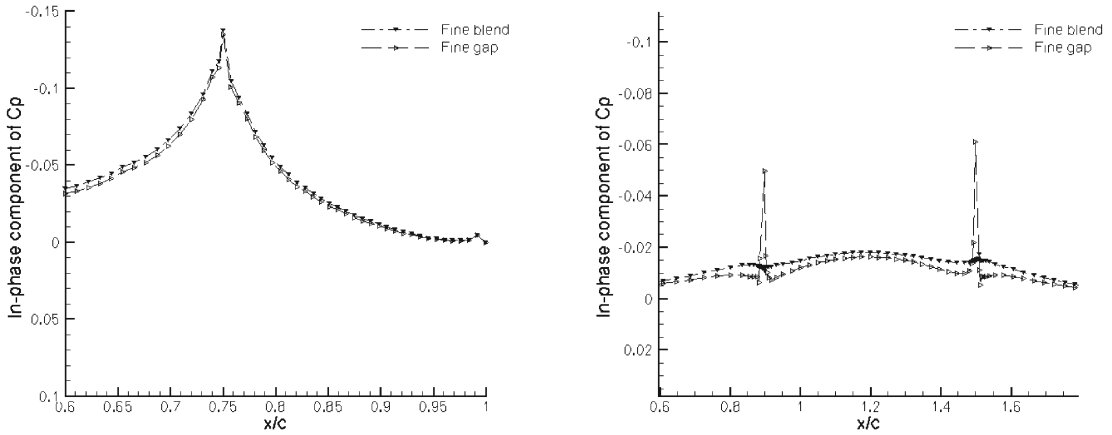

c) In-phase component - streamwise

d) In-phase component - spanwise

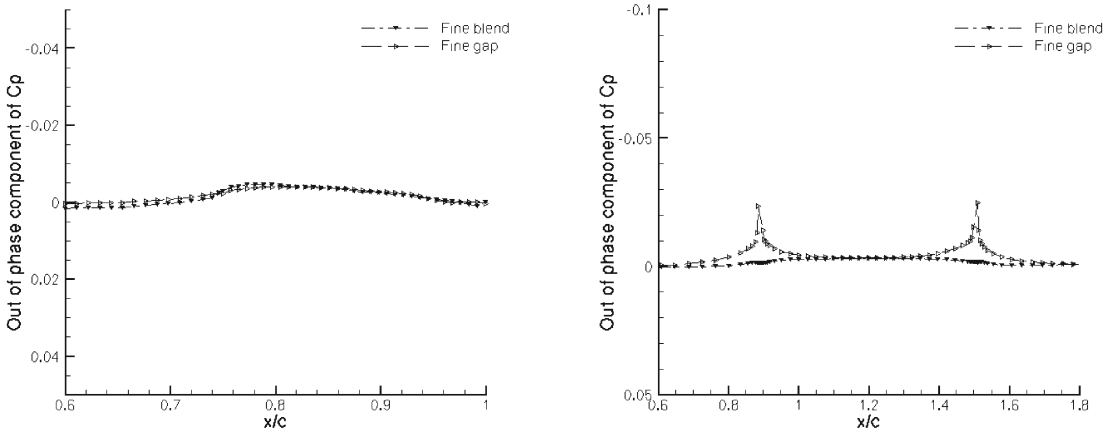

e) Out-phase component - streamwise

f) Out-phase component - spanwise

Fig. 6 BACT case 3 detail around the flap. Comparison between the blended and gap treatment. $M_\infty = 0.769$, $Re = 3.96 \times 10^6$, $\delta_f = 2.0$ deg, FOF 5 Hz.

aft of this point at all FOFs. The dynamic deformation is obtained along a line originating at the wing root which is at 8% semispan including the fuselage, and 80.7% of the root chord. The line makes an angle of 113 deg with the x axis. The Reynolds number based on root chord for the cases selected for calculation is approximately 21.4×10^6.

Along with the measured unsteady pressure and deformation, the finite element model (FEM) data in the form of a structural grid and computed natural modes of vibration are also provided in the paper [15]. A brief description of the structure of the experimental model is presented in an earlier paper by Tamayama [16]. The wing structure is made up of a 7 mm thick aluminum plate with holes drilled to make it flexible. It was found in the experiments that the frequency of the first wing bending mode increased from 9.79 Hz in vacuum to around 15 Hz at Mach 0.8 [16]. It was also indicated that the response of the wing in vacuum is much lower than in air, and this has been used to justify neglecting the inertial effect of the flap motion on the wing response. As the frequency of the wing bending mode lies in the vicinity of the forced FOFs (5–30 Hz), and as the frequency of the next natural mode is higher (40.25 Hz), almost all the deformation of the structure is contributed by the first wing bending mode. It was observed in the experiments that this mode stiffened in the flow and resonance was seen at a FOF of 15 Hz. To obtain a good comparison of computed dynamic deformation with the experiments it is required that the first wing bending mode couples at the correct oscillating frequency.

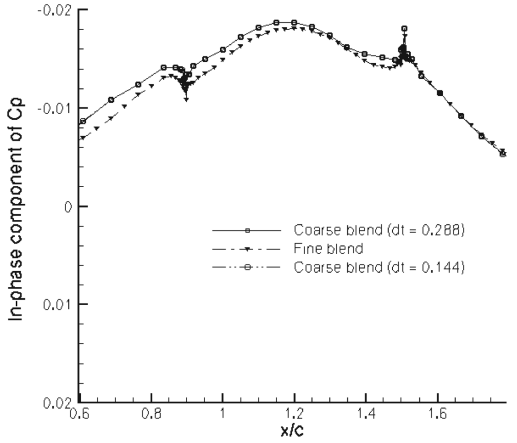

Fig. 7 BACT case 3 detail around the flap. Comparison of in-phase spanwise component between the coarse and fine grids. $M_\infty = 0.769$, $Re = 3.96 \times 10^6$, $\delta_f = 2.0$ deg, FOF 5 Hz.

It was found in the current study that the FEM model provided with the experimental results [15] did not resonate with the FOF of 15 Hz. Closer examination of the structural model presented in [15] showed the presence of an unidentified mode between the first wing bending and torsion modes. To test the stiffening of the original model in the flow an aeroelastic simulation was performed with the given FEM model and the flow conditions described in the experiment [16]. A small impulse was given to the wing and the frequency of the oscillation was calculated. At Mach 0.8 and a dynamic pressure of 23.35 kPa the frequency of the first wing bending mode increased from 11.09 to 12 Hz instead of to 15 Hz as quoted in the experiments. Because of this the resonance between the flap oscillations and the structural modes takes place at a FOF of 10 Hz.

A stiffer model was constructed to remove the unidentified mode. The new stiffer model resonates with a FOF of 15 Hz as in the experiments. Figure 1 shows the structural grid and the first three modes of the stiffened model transformed onto the surface grid. The wing deformations are primarily in the y direction and the y-displacement contours are plotted in the figure. The first three natural modes are included in the aeroelastic calculations described below.

Grids

CFD Grids

BACT Wing

To model the effect of gaps at the flap edges two different grids have been used, with the flap treatment shown in Fig. 2. The first is a RANS grid with blended flap edges. The wall spacing is 1×10^{-6} c on the fine grid which has grid 2.7×10^6 cells. The y+ value is less than 3 across the wing, with a geometric grid stretching ratio of 1.2 normal to the surface. A coarse grid was extracted by removing every alternate grid point in all three directions. The second grid is a RANS grid with free flap edges and is of approximately the same size. A small gap of width 2% of the flap span was introduced between the flap edge and the wing. This gap is filled with a wedge shaped block in the flow domain. The rest of the topology and wall spacings are as for the blended edge. The blocking topology of the grids has a C-type blocking over the wing leading edge and a H-type blocking at the trailing edge. The wing tip is a rotated aerofoil half-profile and the block face over the tip is collapsed into an edge.

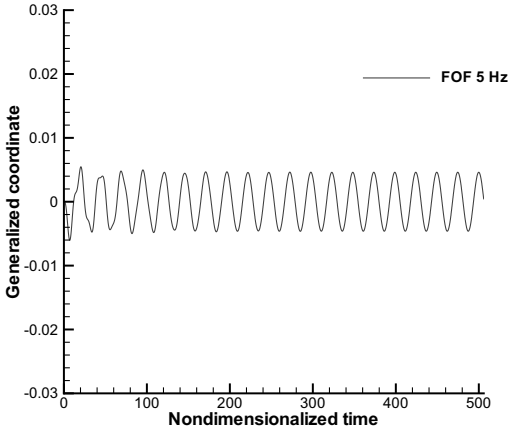

a) FOF 5 Hz

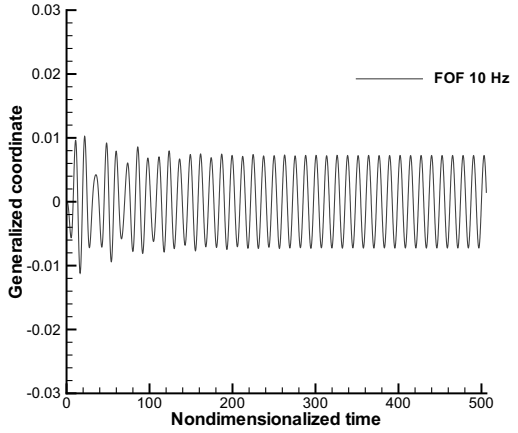

b) FOF 10 Hz

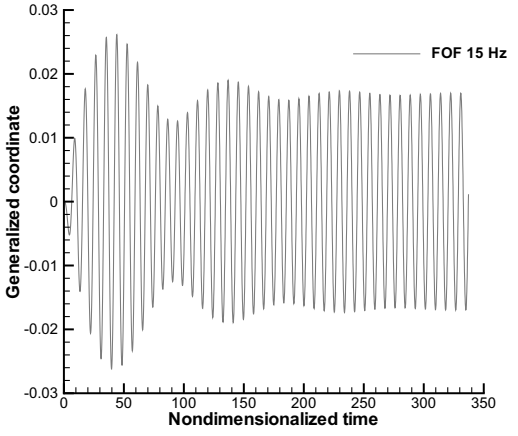

c) FOF 15 Hz

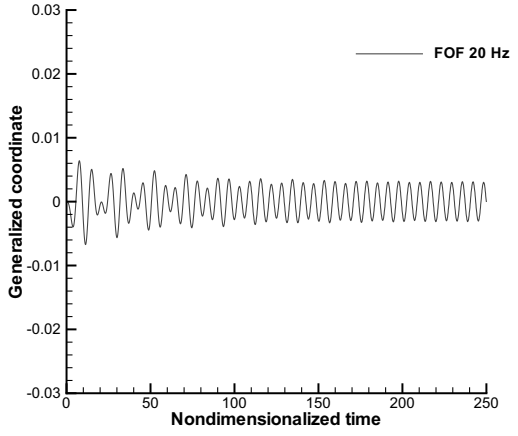

d) FOF 20 Hz

Fig. 8 Wing bending modal coordinate response to different flap frequencies for SST case 1 using the Euler simulation on the coarse grid.

NAL–SST Arrow Wing

To model the effect of gaps and viscosity, four different grids have been used in this work. The RANS grid has 15 cells to resolve the boundary layer, with a y+ of less than 3 and a geometric grid stretching of 1.1. The wall spacing is 1.8×10^{-6} c. The RANS calculations are performed only with blended flaps. A C-type grid topology is used over the wing leading edge, the wing tip, and also around the fuselage. The blocks at the trailing edge are of H-type. Points are clustered around the trailing edge and the flap region where a shock is likely to develop and move. There are 14 cells in the chordwise direction and 28 in the spanwise direction on the flap. The size of the RANS grid is 800 k cells.

Blended flap Euler grids used the same topology as the viscous grid. The fine Euler grid has 1.6×10^6 cells. There are 24 cells in the chordwise direction and 50 spanwise on the flap. The wall spacing is 1×10^{-3} c. A coarse grid is obtained from the fine grid by removing every alternate grid point in all three directions. The grid used for flaps with gaps is similar to the coarse Euler grid for blended flaps but with two extra blocks in the gaps between the flap edges and the wing.

BACT Results

Case 1 provides a good starting point to test the grid treatment and the ability to predict the mild shock that forms. Case 2 has a static flap deflection of 5 deg which tests the shearing of the cells in the gap region between the flap and wing edge. Case 3 is the dynamic case with 0 deg incidence and no mean flap deflection. As the BACT case is a rigid test case the effect of wing flexibility on the aerodynamics is absent.

First we consider the comparisons with measurements before looking closer at the behavior around the flap. The steady cases 1 and 2 show good comparisons with the measurements for the steady pressure coefficient, as shown in Fig. 3. These results are on the coarse grid and there is practically no visible difference from the blended treatment compared with the simulation including a gap at the flap edge. Figure 4 shows the mean and unsteady computed and experimental pressure coefficient (Cp) for the unsteady case 3 at 40 and 60% span. The unsteady calculation on the RANS grid with 800,000 cells was run on four 3 GHz processors, using 200 time steps per cycle and around 20 subiterations per real time step. The computation of four cycles took around one day, a timing which was not very sensitive to the blending or gap flap treatment.

The global behavior on the wing appears to be well represented by the blended flap treatment. Next we look in more detail at the behavior around the flap. Pressure distributions are considered on two slices shown in Fig. 5, referred to as streamwise and spanwise. The mean and unsteady pressure distributions along these slices are shown in Fig. 6 for case 3 using the blended and edge treatments on the fine grids. For the streamwise slice there is very little difference seen between the two treatments. The spanwise slice shows differences when it passes through the edge, with the gap treatment showing a spike of unsteadiness due to flow through the gap. A zoom of the in-phase pressure coefficient comparison around the flap edge for the blended treatment and the two grids and time steps is shown in Fig. 7. This shows that the two time steps are in perfect agreement and that the coarse grid solution agrees well with the fine grid solution using the blended flap treatment.

SST Results

Next we look to the SST test case which introduces flexibility. Figure 8 shows the first wing bending mode history for case 1 for different flap oscillation frequencies. At the FOF of 15 Hz there is

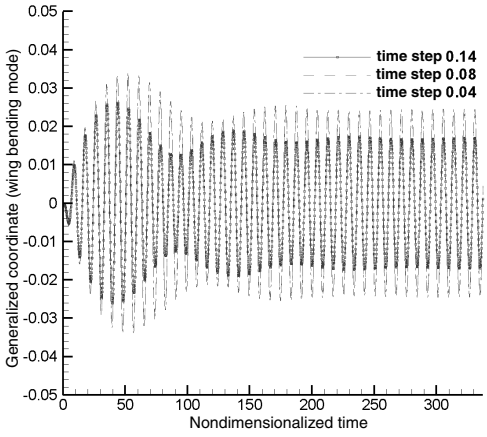

a) Time Step study at FOF of 15 Hz

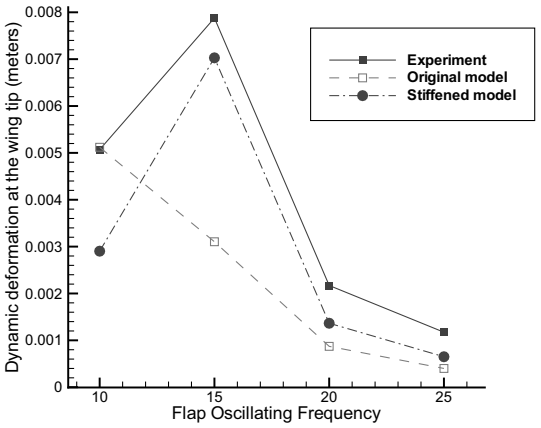

b) Comparison of dynamic tip deformation

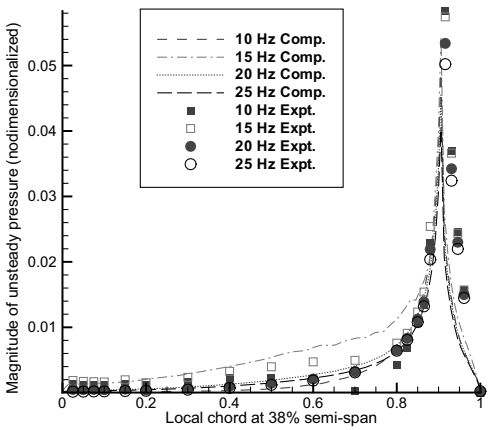

c) Unsteady pressure at 38% semispan location

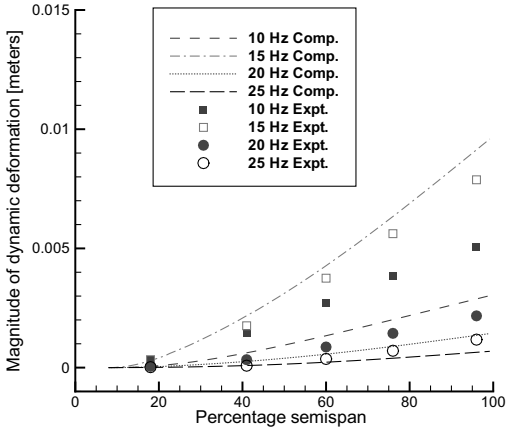

d) Unsteady deformation along the span

Fig. 9 Results for the SST case 1 using the Euler simulation on the coarse grids.

coupling between the first structural mode and the flap oscillations, resulting in a significantly larger deformation of the structure.

Evaluation of the case 1 solution is made in Fig. 9. First, a time step study is shown in Fig. 9a, where the bending mode response for the FOF of 15 Hz is compared for reduced time steps of 0.14, 0.08, and 0.04. The smaller time steps show good agreement, and a time step of 0.08 was used for the remaining calculations, corresponding to around 100 steps per cycle. The time step for the cases off resonance which was required for time accuracy was found to be larger. For the Euler calculations on the 1.6×10^6 grid, six processors were used to calculate 2400 time steps, with around 10 subiterations per real time step, and this took 60 h of wall clock time.

Next, the comparison of the tip deflections for the original and modified structural models is compared with measurements in Fig. 9b. The resonance at the FOF of 15 Hz for the modified model is clear from the plot and shows good agreement with the measurements.

Figures 9c and 9d show the magnitude of the unsteady pressure, and deformation in meters, on a coarse grid using the Euler equations for various FOF. Blended flap edges are used in these simulations. The computed unsteady pressure and deformation compare well with measurements, especially at the resonant FOF of 15 Hz. The position and magnitude of the pressure peaks over the flap at 38% semispan are well predicted for all FOFs. The dynamic deformation magnitude peaks at the resonant FOF frequency of 15 Hz.

Next case 2 is considered. Figures 10a and 10b show the magnitude of the unsteady pressure, and deformation in meters, on a coarse grid using the Euler equations for various FOF. Conclusions are similar to case 1. Again the blended flap was used for these results. Coarse grid blended results are compared with the coarse and fine grid results for the edge gap at the FOF of 15 Hz in Figs. 10c and 10d. First, the coarse and fine results for the gap treatment agree well. Secondly, the blended and gap results are also in good agreement.

Finally case 3 is considered. At the higher freestream Mach number and angle of incidence the shock is located just aft of the flap hinge and the peak unsteadiness is much higher than in cases 1 and 2. Figures 11a and 11b again show the magnitude of the unsteady pressure, and deformation in meters, on a coarse grid using the Euler equations for various FOF. Conclusions are similar to cases 1 and 2, although the peak unsteadiness is now overpredicted, an effect which is sensitive to the mean prediction of the shock wave. Figures 11c and 11d show a comparison of the Euler and RANS results for this case. The RANS results locate the shock wave slightly upstream of the Euler result in better agreement with the measurements, and the peak magnitude of the unsteady pressure coefficient is smaller, again in better agreement with the measurements. A close-up of the region around the flap hinge is shown in Fig. 11e which illustrates these points more clearly.

The details around the flap are now considered in Fig. 12. Again the pressure distributions are shown along two slices defined in Fig. 12a. The mean and magnitude of the unsteady pressure coefficient are shown along the streamwise and spanwise slices. The Euler results from the coarse and fine grids using the blending treatment and the coarse grid with the gap are compared. First, on the streamwise slice all three results are very close. Of more interest is the spanwise slice which goes through the flap edges. The mean values shown in Fig. 12c all agree well. There is some difference in the unsteady pressure coefficient magnitudes, shown in Fig. 12e. The fine results show a higher value than the coarse grid. The grid with the gap shows a lower level of unsteadiness with again a spike around the

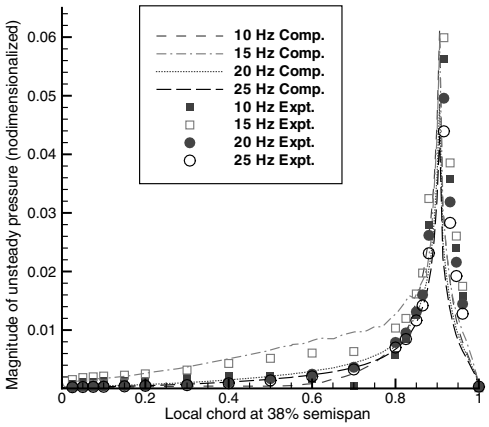

a) Unsteady pressure at 38% semispan location on coarse grid

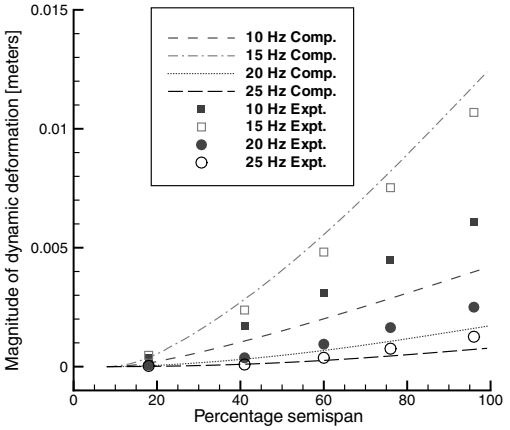

b) Unsteady deformation along the span on coarse grid

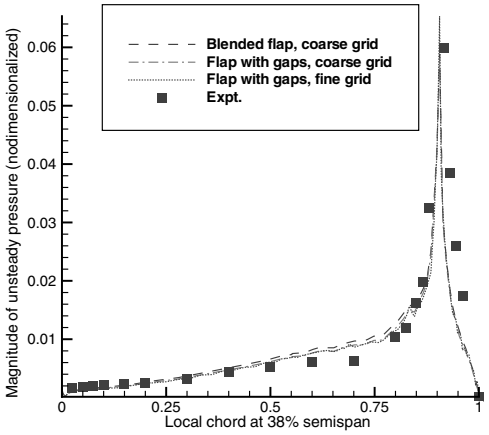

c) Unsteady pressure at 38% semispan location - grid refinement for FOF of 15Hz

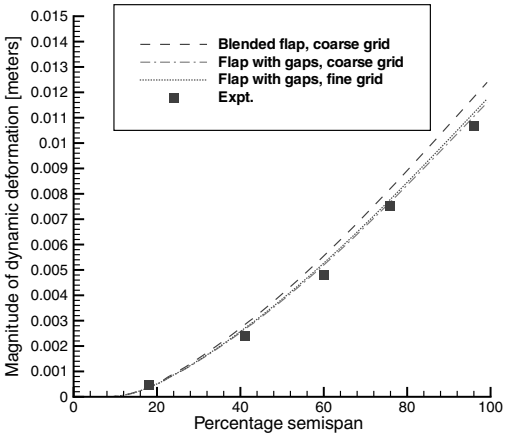

d) Unsteady deformation along the span - grid refinement for FOF of 15Hz

Fig. 10 Unsteady pressure and deformation plots for the SST case 2 using the Euler solution.

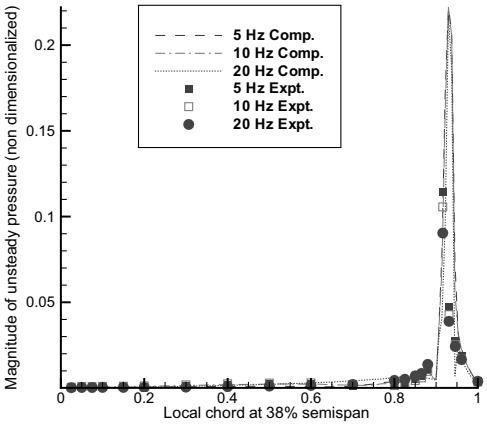

a) Unsteady pressure at 38% semispan location from the Euler solutions on the coarse grid

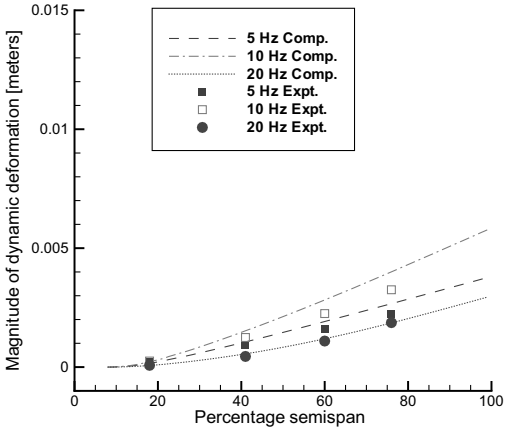

b) Unsteady deformation along the span from the Euler solutions on coarse grid

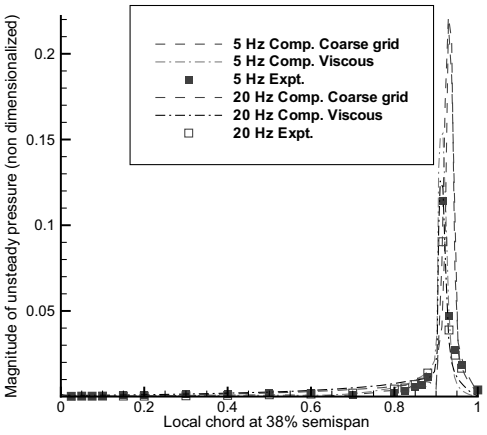

c) Unsteady pressure at 38% semispan location - RANS solutions on the coarse and fine grids

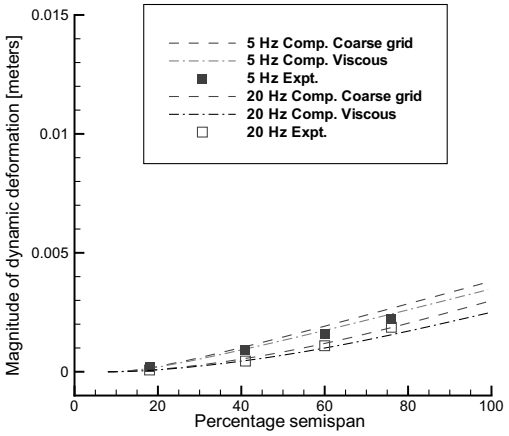

d) Unsteady deformation along the span - RANS solutions on the coarse and fine grids

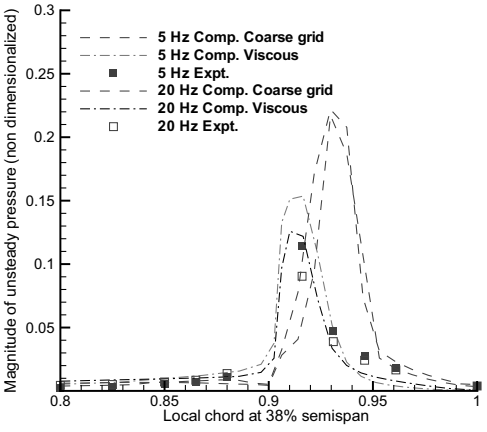

e) Unsteady pressure at 38% semispan location - RANS solutions on the coarse and fine grids. Zoom in on flap hinge region

Fig. 11 Unsteady pressure and deformation plots for the SST case 3 using the Euler and unsteady Reynolds averaged Navier–Stokes (URANS) solutions.

flap edge, suggesting that the flow through the gap provides some alleviation of the pressure changes due to the flap motion.

Conclusions

Unsteady viscous and inviscid forced flap oscillation simulations were performed on the flexible NAL–SST arrow wing and the rigid BACT wing using a range of FOFs. A good comparison is obtained of the steady and unsteady surface pressures with the experiments for the BACT case. The pressure unsteadiness is predominantly in-phase with the flap oscillations as the Fourier processed out-of-phase component is very small compared to the in-phase component.

The predicted dynamic deformation of the SST compares well with the experiments at the resonant frequency and a reasonable comparison for unsteady pressure distribution was obtained for all frequencies. Viscous effects were found to be negligible and inviscid predictions were as accurate as viscous for the case with 0 deg incidence. As expected, the Euler equations can accurately predict

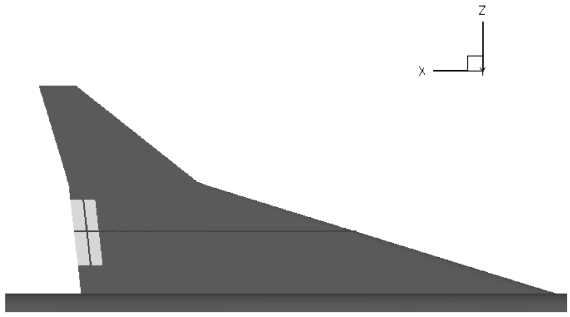

a) Definition of slices

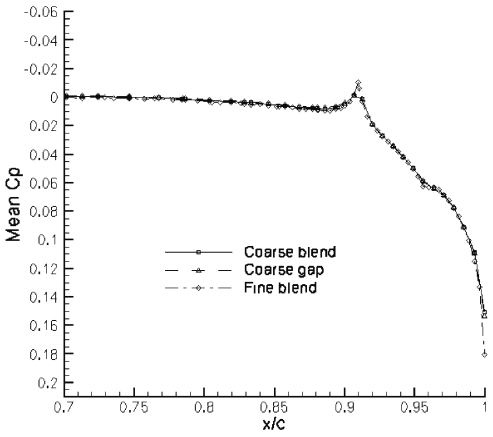

b) Mean - streamwise

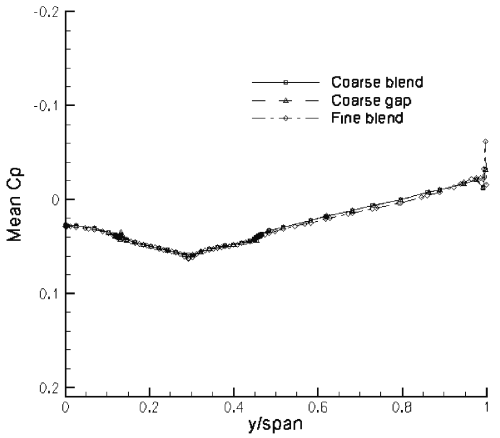

c) Mean - streamwise

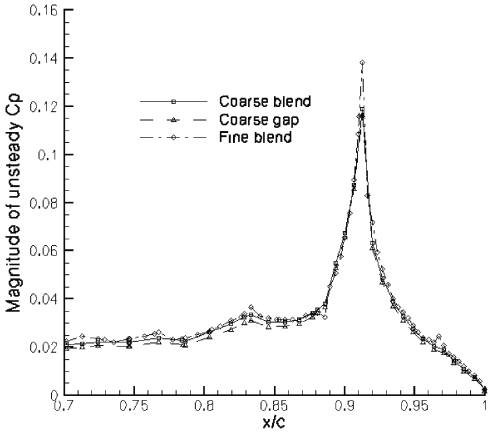

d) Unsteady magnitude - streamwise

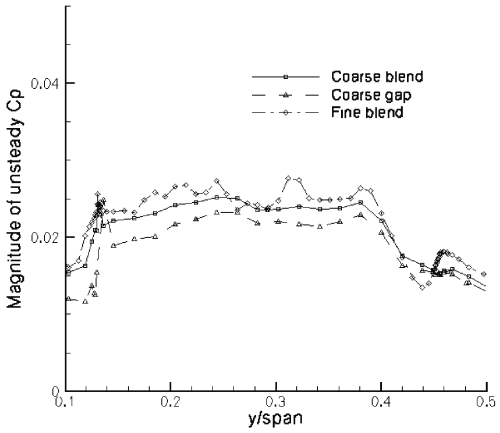

e) Unsteady magnitude - streamwise

Fig. 12 SST case 2 mean and unsteady pressure coefficient values around the flap. $M_\infty = 0.8$, Euler, $\alpha = -2.0$ deg, FOF 15 Hz.

the unsteady pressure for transonic Mach numbers where the shock remains well ahead of the control surface hinge.

The effect of blended flap edges on the prediction of global pressure distribution and deformation of the wing was found to be insignificant when compared with flaps with free edges. However, some differences were seen locally around the flap with flow through the open gap leading to an increase in unsteadiness around the flap edge.

In conclusion, the blended flap provides a straightforward grid treatment which has proved capable for representing global structural response of the SST test case.

Acknowledgments

This work was supported by BAE SYSTEMS, Engineering and Physical Sciences Research Council, Department of Trade and Industry and Ministry of Defence, and is part of the work program of the Partnership for Unsteady Methods in Aerodynamics (PUMA) Defence and Aerospace Research Partnership (DARP).

References

[1] Erickson, A. L., and Stephenson, J. D., "A Suggested Method for Analyzing for Transonic Flutter of Control Surfaces Based on Available Data," NACA RM A7F30, 1947.

[2] Lambourne, N. C., "Control Surface Buzz," Aircraft Research Council R & M, No. 3364, 1964.

[3] Brase, L. O., Fuglsang, D. F., and Agarwal, S., "A Numerical Study of Control Surface Buzz Using Computational Fluid Dynamics Methods," AIAA Paper 92-2654, June 1992.

[4] Livne, E., and Weisshaar, T., "Aeroelasticity of Nonconventional Airplane Configurations—Past and Future," *Journal of Aircraft*, Vol. 40, No. 6, 2003, pp. 1047–1065.

[5] Abzug, M., and Larrabee, E., *Airplane Stability and Control—A History of Technologies That Made Aviation Possible*, Cambridge Univ. Press, Cambridge, England, U. K., 1997, Chap. 19.

[6] Bharadvaj, B. K., "Computation of Steady and Unsteady Control Surface Loads in Transonic Flow," AIAA Paper 90-0935, 1990.
[7] Schuster, D. M., and Bartels, R. E., "Benchmark Active Control Technology (BACT) Wing CFD Results," *Verification an Validation Data for Computational Unsteady Aerodynamics*, RTO TR 26, Oct. 2000, pp. 225–238.
[8] Cole, H. S., Andrew, A. S., and Gupta, K., "Application of the Transpiration Method for Aeroservoelastic Prediction Using CFD," AIAA Paper 98-2071, 1998.
[9] Cole, H. S., Andrew, A. S., and Gupta, K., "CFD-Based Aeroservoelastic Predictions with Comparisons to Benchmark Experimental Data," AIAA Paper 99-0766, Jan. 1999.
[10] Klopfer, G., and Molvik, G., "Conservative Multizonal Interface Algorithm for the 3-D Navier–Stokes Equations," AIAA Paper 93-1601, 1991.
[11] Klopfer, G., and Obayashi, S., "Virtual Zone Navier-Stokes Computations for Oscillating Control Surfaces," AIAA Paper 93-3363, 1993.
[12] Obayashi, S., and Guruswamy, G., "Navier-Stokes Computations for Oscillating Control Surfaces," AIAA Paper 92-4431, 1992.
[13] Obayashi, S., Chiu, I. T., and Guruswamy, G., "Navier-Stokes Computations on Full Span Wing Body Configuration for Oscillating Control Surfaces," AIAA Paper 93-3687, 1993.
[14] Karlsson, A., and Winzell, B., "Unsteady Control Surface Pressure Measurements and Computations," AIAA Paper 96-2417, 1996.
[15] Matsushita, H., Tamayama, M., Saitoh, K., and Nakamichi, J., "NAL SST Arrow Wing with Oscillating Flap," *Verification an Validation Data for Computational Unsteady Aerodynamics*, RTO TR 26, Oct, 2000, pp. 295–318.
[16] Tamayama, M., and Nakamichi, J., "Unsteady Aerodynamics Measurements on an Elastic Wing Model of SST," AIAA Paper 97-0836, Jan. 1997.
[17] Weisshaar, T. A., Tamayama, M., and Nakamichi, J., "Unsteady Shock Wave Motions on a Thin Airfoil at Transonic Speeds Caused by an Aileron Oscillation," *International Forum on Aeroelasticity and Structural Dynamics—Amsterdam*, AIAA, Reston, VA, 4–6 June 2003.
[18] Utaka, Y., and Nakamichi, J., "Aeroelastic Analysis of an SST Typed Wing with a Trailing Edge Flap Using a Chimera Grid Approach," AIAA Paper 2004-1271, 2004.
[19] Osher, S., and Chakravarthy, S., "Upwind Schemes and Boundary Conditions with Applications to Euler Equations in General Geometries," *Journal of Computational Physics*, Vol. 50, No. 3, 1983, pp. 447–481.
[20] Jameson, A., "Time Dependent Calculations Using Multigrid, with Applications to Unsteady Flows Past Airfoils and Wings," AIAA Paper 1991-1596, June 1991.
[21] Badcock, K. J., Woodgate, M. A., and Richards, B. E., "Elements of Computational Fluid Dynamics on Block Structured Grids Using Implicit Solvers," *Progress in Aerospace Sciences*, Vol. 36, Nos. 5–6, 2000, pp. 351–392.
[22] Gordon, W. J., and Hall, C. A., "Construction of Curvilinear Coordinate Systems and Applications to Mesh Generation," *International Journal of Numerical Methods in Engineering*, Vol. 7, No. 4, 1973, pp. 461–477.
[23] Thomas, P., and Lombard, C., "Geometric Conservation Law and Its Application to Flow Computations on Moving Grids," *AIAA Journal*, Vol. 17, No. 10, 1979, pp. 1030–1037.
[24] Goura, G. S. L., "Time Marching Analysis of Flutter Using Computational Fluid Dynamics," Ph.D. Thesis, University of Glasgow, Glasgow, U.K., 2001.
[25] Scott, R. C., Bennett, R. M., and Wieseman, C. D., "Test Cases for the Benchmark Active Controls Model: Spoiler and Control Surface Oscillations and Flutter," *Verification an Validation Data for Computational Unsteady Aerodynamics*, RTO TR 26, Oct. 2000, pp. 201–224.
[26] Rampurawala, A. M., "Aeroelastic Analysis of Aircraft with Control Surfaces using CFD," Ph.D. Thesis, University of Glasgow, Glasgow, U.K., 2006.